Near spherical shell-model structure of the 2_1^+ state in ^{40}Ar from *g*-factor measurements

E. A. Stefanova,[1,*] N. Benczer-Koller,[1] G. J. Kumbartzki,[1] Y. Y. Sharon,[1] L. Zamick,[1] S. J. Q. Robinson,[2] L. Bernstein,[3] J. R. Cooper,[3] D. Judson,[4] M. J. Taylor,[4] M. A. McMahan,[5] and L. Phair[5]

[1]*Department of Physics and Astronomy, Rutgers University, New Brunswick, New Jersey 08903, USA*

[2]*Department of Geology and Physics, University of Southern Indiana, Evansville, Indiana 47712, USA*

[3]*Lawrence Livermore National Laboratory, Livermore, California 94551, USA*

[4]*School of Engineering, University of Brighton, Brighton BN2 4GJ, United Kingdom*

[5]*Lawrence Berkeley National Laboratory, Berkeley, California 94720, USA*

(Received 1 September 2004; published 21 July 2005)

The *g* factor of the 2_1^+ state in ^{40}Ar has been measured by use of Coulomb excitation in inverse kinematics and the transient magnetic-field technique. The resulting *g* factor, $g(2_1^+) = -0.015(42)$, is in reasonable agreement with shell-model calculations within the (full $sd)_\pi$(full $fp)_\nu$ space, without including core excitations. Although highly deformed admixtures in the wave function cannot be completely ruled out, they are small, in contrast to the case of ^{42}Ca.

DOI: 10.1103/PhysRevC.72.014309 PACS number(s): 21.10.Ky, 25.70.De, 27.50.+e

I. INTRODUCTION

The nucleus ^{40}Ar straddles the *sd* proton and the *fp* neutron shells. ^{40}Ar has the same number of neutrons as ^{42}Ca but it has two proton holes in the *sd* shell. The *fp* nuclei have been extensively studied, and many shell-model calculations have been carried out, for example, in Refs. [1–6] and references therein. Among them, the Ca isotopes between $^{40}_{20}$Ca$_{20}$ and $^{48}_{20}$Ca$_{28}$, although widely investigated in the past, are still a challenge for theory. Recently, positive values of $g(2_1^+, ^{42}\text{Ca}) = +0.04(6)$ [7] and $g(2_1^+, ^{44}\text{Ca}) = +0.12(5)$ [8], $+0.17(3)$ [7] have been measured. These values disagree with those of the pure $f_{7/2}$ or *fp* neutron configurations expected from simple shell-model considerations, which would result in negative *g* factors. Complete *fp* calculations predict negative values for *g*, –0.3 to –0.5 [7,8]. Thus the experimental *g* factors reveal a strong contribution from ^{40}Ca core excitations to the wave functions of the 2_1^+ states in ^{42}Ca and ^{44}Ca. This issue was actually discussed about 40 years ago [9,10], when it was suggested that the 2_1^+ states in ^{42}Ca and ^{44}Ca are mixtures of spherical shell-model and deformed core configurations. By use of the same Gerace and Green approach [9] and the measured *g* factors, core-deformed components of 55(6)% and 65(4)% were estimated for the 2_1^+ states of ^{42}Ca and ^{44}Ca, respectively [7,8]. However, the two negative values, $g = -0.19(12)$ and $g = -0.26(6)$, measured for the 2_1^+ state in ^{46}Ca [11,12], require a small or no core-excitation component.

In light of the structure of the Ca isotopes just discussed, questions arise about ^{40}Ar, the isotone of ^{42}Ca. How does the residual interaction depend on the number of *sd* shell proton holes? Do core excitations play as important a role as in ^{42}Ca?

The *g* factor of the $^{40}\text{Ar}(2_1^+)$ state had been measured before [13], also by the transient field technique but with very high-velocity ^{40}Ar projectiles ($v/v_0 = 19$) and a ^{208}Pb target. The measured *g* factor was $g = -0.1(1)$ [13], a result which indicates a complex interplay of neutron and proton configurations. A new measurement of the $^{40}\text{Ar}(2_1^+)$ *g* factor, using Coulomb excitation in inverse kinematics and the transient field technique at low energies, would not only provide a confirmation of the previous result but would also shed light on the transient field parametrization for very high velocities. This paper reports on such a new measurement.

II. EXPERIMENTAL TECHNIQUE

In this experiment ^{40}Ar was Coulomb excited in inverse kinematics by a light C target, and the *g* factor of the 2_1^+ state was measured by the transient field technique as described in recent publications [14–16].

A beam of ^{40}Ar was accelerated at the Lawrence Berkeley National Laboratory 88-Inch Cyclotron to an energy of 80 MeV. A multilayer target was used, consisting of 0.42 mg/cm^2 of natural carbon evaporated on 0.005-mg/cm^2 titanium deposited on a 3.24-mg/cm^2 gadolinium layer, itself evaporated on a 1.40-mg/cm^2 tantalum foil and backed by a copper layer of 3.54 mg/cm^2. An additional copper layer of 5.60 mg/cm^2 was added to ensure that the beam was completely stopped in the target. The preparation of the ferromagnetic gadolinium foil is described in Ref. [17]. The target was kept at ≈ 100 K by a liquid-nitrogen reservoir. The temperature was monitored with a thermocouple connected to the target frame. An external magnetic field of 0.06 T was applied in a direction perpendicular to the γ-ray detection plane, and its direction was reversed every 4 min. The target magnetization was measured with an ac magnetometer [18] to be $\vec{M} = 0.1726$ T at the temperature and external field used during the experiment.

The ^{40}Ar projectiles, excited into the 2_1^+ state, traverse the polarized ferromagnetic gadolinium layer, where they experience spin precession in the transient hyperfine magnetic field. The excited ^{40}Ar ions are then stopped and decay in the copper backing, a region free of hyperfine interactions. The

[*]Permanent address: Institute for Nuclear Research Nuclear Energy BAS, BG-1784 Sofia, Bulgaria.

TABLE I. Kinematics of the excited ^{40}Ar and ^{46}Ti projectiles traversing the ferromagnetic layer. θ_p is the maximum acceptance angle for carbon recoils into the Si particle detector for two different geometries. $\langle E\rangle_{\rm in}$ and $\langle E\rangle_{\rm out}$, $\langle v/v_0\rangle_{\rm in}$ and $\langle v/v_0\rangle_{\rm out}$ are, respectively, the average energies and velocities of the excited ions as they enter into, and exit from, the gadolinium layer; $v_0 = e^2/\hbar$ is the Bohr velocity. $\langle\Delta t\rangle$ is the average traversal time of the ions through the gadolinium layer.

Nucleus	$E_{\rm beam}$ (MeV)	θ_p (deg)	$\langle E\rangle_{\rm in}$ (MeV)	$\langle E\rangle_{\rm out}$ (MeV)	$\langle\frac{v}{v_0}\rangle_{\rm in}$	$\langle\frac{v}{v_0}\rangle_{\rm out}$	$\langle\Delta t\rangle$ (ps)
^{40}Ar	80	22.4	21.7	2.6	4.7	1.6	0.52
	80	10	18.2	1.6	4.3	1.3	0.59
^{46}Ti	100	22.4	31.3	5.4	5.2	2.2	0.53

carbon recoils leave the target and are detected in a silicon particle detector, centered at 0° relative to the beam axis and subtending an angle of 22.4° with respect to the beam. The kinematics of the excited Ar ions as they enter into, and exit from, the gadolinium layer were calculated with the Ziegler *et al.* [19] stopping powers and are summarized in Table I. The γ rays were detected with four Clover Ge detectors. The distance between the target and the face of the Clover detectors' enclosure was 12.2 cm. Only γ rays in coincidence with C recoils were recorded. In addition, the kinematics of a complementary calibration experiment carried out with a ^{46}Ti beam, the same target, and the same geometrical conditions are given in Table I. This experiment was performed at higher beam energies to achieve enough yield.

The low-lying levels in ^{40}Ar, taken from Ref. [20], are shown in Fig. 1. The γ-ray spectrum collected during the

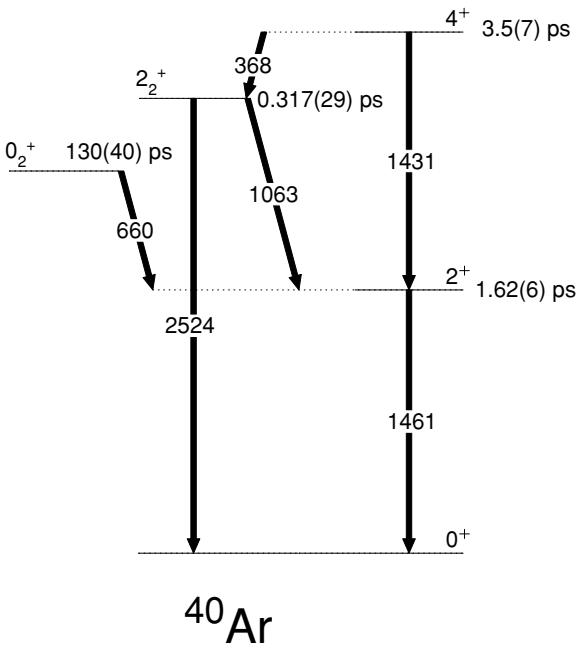

FIG. 1. The low-energy part of the level scheme of ^{40}Ar, taken from [19]. The mean lifetimes of the states, also taken from [19], are given next to them. The energies are given in keV.

precession measurement with a Clover detector at 113°, and sorted with coincidence conditions on the time and total recoil-carbon particle spectrum, is shown in Fig. 2, with random counts subtracted and with Compton add-back included. Many contamination lines appear in the spectrum, because the reaction was done at ∼10 MeV above the Coulomb barrier where fusion-evaporation and stripping-pickup reactions compete with Coulomb excitation. The strongest contamination channel is ^{12}C(^{40}Ar,αn)^{47}Ti.

Figure 3(a) shows the particle spectrum we obtained in coincidence with all γ rays. Figure 3(b) shows the particle spectrum we obtained by requiring a coincidence with the photopeak of the 1461-keV γ ray. The sharp features observed correspond to α particles. For example, a similar particle spectrum we obtained by gating with γ rays belonging to ^{47}Ti yields only the sharp α peaks. Figure 3(c) shows the spectrum we obtained after subtracting from the spectrum in Fig. 3(b) the particle spectrum we obtained in coincidence with the γ-ray background around the 1461-keV line. Only C recoils remain.

A line at an energy of 1431 keV, which is exactly the energy of the $4_1^+ \rightarrow 2_1^+$ transition in ^{40}Ar (Fig. 1) was observed (see Fig. 2). Its intensity is ∼18% of the intensity of the $2_1^+ \rightarrow 0_1^+$ 1461-keV transition, whereas the COULEX calculations [21] predict the population of the 4_1^+ state to be only ∼0.12% of the population of the 2_1^+ state. A transition at 1431 keV was observed in ^{47}Ti in Refs. [1,22]. It was ∼3% of the intensity of the strongest line at 159 keV in ^{47}Ti in [1], ∼7% in [22], and ∼7% in the present experiment. Thus one may conclude that the 1431-keV line belongs to ^{47}Ti. In addition, it can be seen from Fig. 2 that the backward Doppler-shifted tail of the 1461-keV $2_1^+ \rightarrow 0_1^+$ transition slightly overlaps with this 1431-keV line.

A γ-ray spectrum obtained by gating with only high-energy C recoils (above channel 400) results in an extremely clean ^{40}Ar spectrum (Fig. 4) showing only the $2_1^+ \rightarrow 0_1^+$ transition. The high-energy C recoils correspond to C ions detected within 0° to ∼10°, whereas the whole spectrum of C recoils corresponds to detection of the C within the whole 22.4° aperture subtended by the particle detector. These two different spectra were used in the analysis described in the next section.

III. DATA ANALYSIS

In general, the g factor of an excited short-lived (about a few picoseconds) state can be deduced by measurement of the precession angle of its magnetic moment, $\Delta\theta = \epsilon/S$, in the transient hyperfine magnetic field. The quantity ϵ denotes the "effect" of the spin precession in the external field and is defined more precisely below, and S is the logarithmic slope of the particle-γ angular correlation at the γ-ray detector angles, $S(\theta_\gamma) = [1/W(\theta_\gamma)][dW(\theta_\gamma)/d\theta]$.

The logarithmic slope S is determined from the anisotropy ratios of counts in both γ detector pairs (1,4 and 2,3) placed at different angles. The two forward Clover detectors (2,3) were placed, alternatively, at angles of ±50° and ±80°, whereas the backward Clover detectors (1,4), respectively, were at ±130°

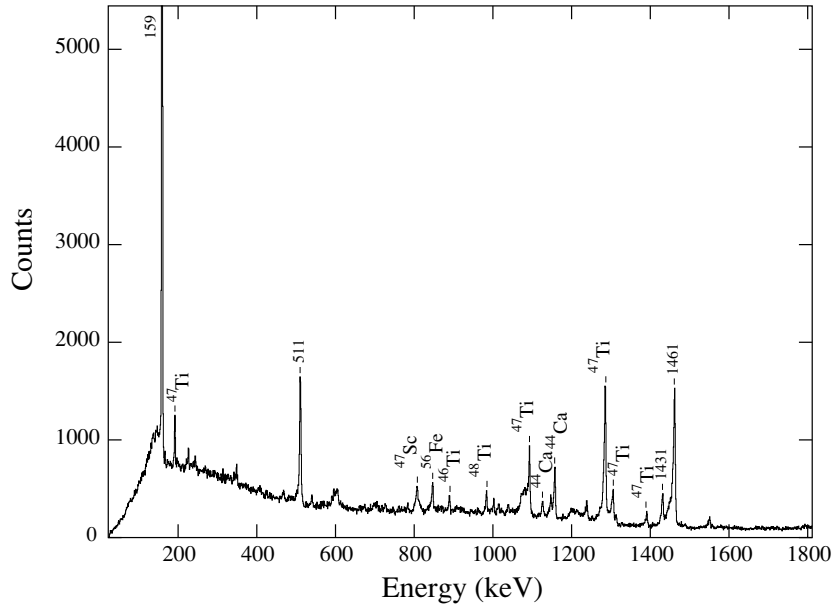

FIG. 2. Coincident particle-γ spectrum from a detector at 113°, collected during the precession measurement and sorted with cuts on the true time and on the whole spectrum of C recoils. It can be seen that the backward Doppler-shifted tail of the 1461-keV line of interest slightly overlaps with a 1431-keV transition in ^{47}Ti. There are many contaminant lines in the spectrum, the strongest coming from the ^{12}C(^{40}Ar,αn)^{47}Ti fusion-evaporation channel. The ^{47}Ti 159-keV line has a maximum intensity of about 20 000 counts.

and $\pm 100^\circ$ with respect to the beam axis:

$$R_{1,4} = \sqrt{\frac{N_1(130^\circ)}{N_1(100^\circ)}\frac{N_4(-130^\circ)}{N_4(-100^\circ)}},\ R_{2,3} = \sqrt{\frac{N_2(50^\circ)}{N_2(80^\circ)}\frac{N_3(-50^\circ)}{N_3(-80^\circ)}}$$

This procedure involves two different measurements with an exchange of the angles of detectors 1 and 4 as well as 2 and 3. For the final result, both anisotropy ratios are averaged. The details of the procedure are described in Refs. [16,23], where it is shown how the angular correlation coefficients $A_2^{\exp}$ and $A_4^{\exp}$ are obtained from the anisotropy ratio R.

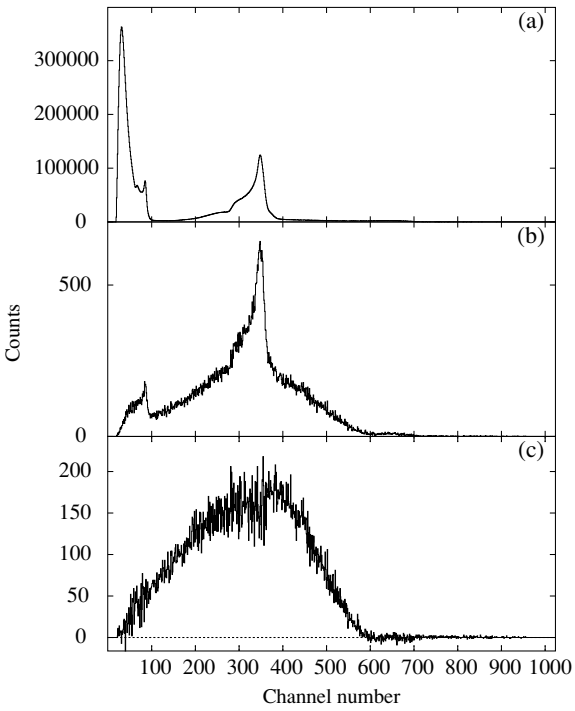

FIG. 3. (a) Particle spectrum in coincidence with all γ rays; (b) particle spectrum in coincidence with the 1461-keV γ-ray line; (c) this spectrum shows a pure C spectrum obtained after we subtracted from (b) the spectrum we obtained by requiring a coincidence with background γ rays around the 1461-keV line.

In the present experiment we measured the spin precession effect ϵ by setting the four detectors at $\pm 67^\circ$ and $\pm 113^\circ$ with respect to the beam axis, angles where the slope is large.

The effect of the precession is given in terms of counting rates by

$$\epsilon = \frac{\rho - 1}{\rho + 1},$$

where

$$\rho = \sqrt{\frac{\rho_{1/4}}{\rho_{2/3}}}, \quad \rho_{i,j} = \sqrt{\frac{N_i^{\uparrow}}{N_i^{\downarrow}}\frac{N_j^{\downarrow}}{N_j^{\uparrow}}},$$

and i, j represents a detector pair; N_i and N_j are the particle-γ coincidence photopeak counts of the γ transition in the ith or jth detector and $\uparrow(\downarrow)$ signifies field "up" ("down").

The ratio ρ, used in the measurement of the effect of precession, and the anisotropy ratios $R_{i,j}$ are constructed so that many systematic errors, such as differences in the beam current, time of measurement, and relative efficiencies of the detectors, cancel out. The g factor can be calculated from

$$\Delta\theta = -g\frac{\mu_N}{\hbar}\int_{t_{\text{in}}}^{t_{\text{out}}} B_{\text{TF}}[v(t),\ Z]e^{-t/\tau}dt, \qquad (1)$$

where B_{TF}, the transient field described by the Rutgers parametrization [24], is a function of the velocity v and atomic number Z of the projectile ion, τ is the mean lifetime of the state of interest, and t_{in} and t_{out} are the mean entrance and exit times of the ions into and out of the ferromagnetic layer, respectively. However, recent experiments on ^{46}Ti ions on the same target [12] have hinted that the Rutgers parametrization may not hold for light nuclei traversing gadolinium foils.

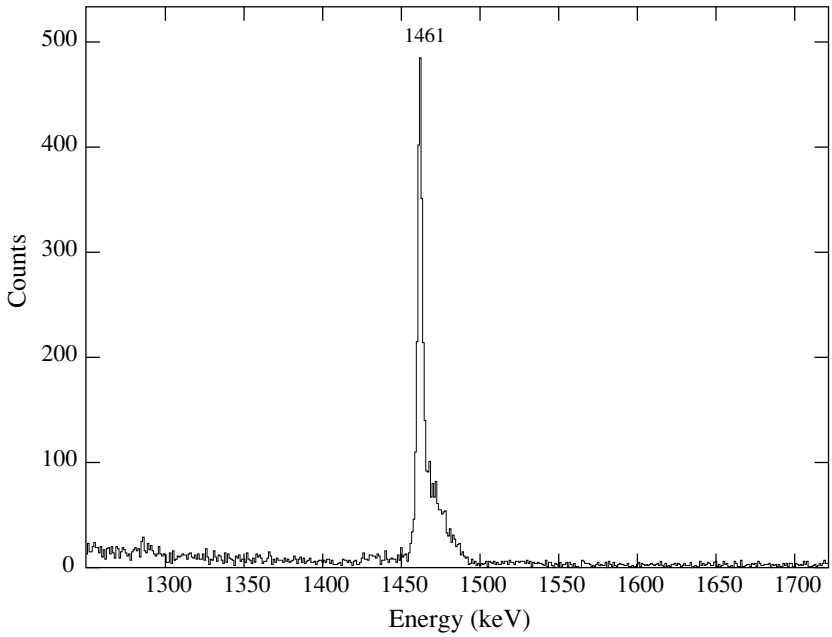

FIG. 4. Coincident particle-γ spectrum from a detector at 67° collected during the precession measurement and sorted with cuts on the true time and only on the high-energy particle spectrum [from channels 400 to 600 in Fig. 3(a)]. It can be seen that the 1431-keV transition is not visible.

Hence, as has been advocated consistently, a calibration of the observed precession $\Delta\theta(^{40}\mathrm{Ar})$ against $\Delta\theta$ of a known magnetic moment in a neighboring nucleus is preferable. The nearest nucleus for which the g factor of the 2_1^+ state is known is ^{46}Ti. A recent measurement, carried out in inverse kinematics on a gadolinium foil and with the Bonn linear parametrization of the transient field [25], yielded $g(2_1^+;^{46}\mathrm{Ti}) = +0.496(27)$. This value agrees with the previous, much less accurate measurement, in forward kinematics, at lower energies, carried out on an iron foil, $g(2_1^+;^{46}\mathrm{Ti}) = +0.49(12)$ [26].

IV. RESULTS

The measured values for R, $S(\theta_\gamma)$ and the g factor for both ^{40}Ar and ^{46}Ti are presented in Table II. The result shown in the first line arises from the analysis of spectra obtained in coincidence with the whole C spectrum for which a weak ^{47}Ti contaminant line at 1431 keV appears below the line of interest. The result shown in the second line is obtained by selection of only the highest-energy C recoils that yielded a ^{40}Ar spectrum free of contaminants.

The first sort yields a g factor of $g(2_1^+) = -0.015(42)$. The second sort results in a clean $^{40}\mathrm{Ar}(2^+ \rightarrow 0^+)$ line, but with reduced statistics, and yields a similar value of $g(2_1^+) = -0.022(54)$. Both results are consistent with each other. They also agree with the previous, high-velocity measurement, $g = -0.1(1)$ [13]. The value of $g(2_1^+) = -0.015(42)$, deduced from the full statistics gained in the present experiment (Table II, sort 1), is chosen as a final result of this experiment. Because the g factor of this state is close to zero, the result is insensitive to any parametrization. For the same reason, no conclusive statement concerning the validity of the transient field at high velocities [13] can be made.

V. DISCUSSION

In the simplest shell-model picture, ^{40}Ar consists of two proton holes in the $d_{3/2}$ orbital and two neutrons in the $f_{7/2}$ orbital. Such a simple shell-model calculation, utilizing a wave function restricted to just two components, $\pi(d_{3/2})_2^{-2}\nu(f_{7/2})_0^2$ and $\pi(d_{3/2})_0^{-2}\nu(f_{7/2})_2^2$, and effective g factors, was reported in Ref. [13]. The result, $g(2_1^+, ^{40}\mathrm{Ar}) = -0.10$, reproduced the measured value of $g = -0.1(1)$ quoted in Ref. [13]. The

TABLE II. Level energy E_x, mean lifetime, the coincidence windows used for different sorts, anisotropy, logarithmic slopes $S(\theta_\gamma)$ of the angular correlations, measured precession angles $\Delta\theta$, and deduced g factors for the 2_1^+ state in ^{40}Ar relative to $g(2_1^+;^{46}\mathrm{Ti})$.

Nucleus	E_x(Mev)	τ (ps)	Sort	$\langle R\rangle$	$\lvert S(67^\circ)\rvert$	$\Delta\theta$ (mrad)	g
^{40}Ar	1.461	1.62(6)	1[a]	3.153(66)	2.50(4)	0.599(1681)	−0.015(42)[b]
			2[c]	3.877(128)	2.86(6)	0.878(2138)	−0.022(54)
^{46}Ti	0.889	8.1(4)[d]		3.10(4)	2.36(3)	−19.8(18)	+0.496(27)[d]

[a] γ spectra sorted with coincidence selection on the total particle spectrum and the true time.
[b] Value adopted from this work.
[c] γ spectra sorted with coincidence selection on the highest-energy particles and the true time.
[d] Ref. [25].

TABLE III. Summary of the shell-model calculations carried out for the 2_1^+ state in ^{40}Ar with the WBT interaction [27], different model spaces, effective charges $e_\pi = 1.5$, $e_\nu = 0.5$, and either the free nucleon g factors $g(s)_\pi = 5.586$, $g(s)_\nu = -3.826$, $g(l)_\pi = 1$, and $g(l)_\nu = 0$, or the effective nucleon g factors $g(s)_\pi = 5.055$, $g(s)_\nu = -3.19$, $g(l)_\pi = 1.06$, and $g(l)_\nu = 0$.

		Model space	$E(2_1^+)$ (MeV)	$B(E2; 0_1^+ \to 2_1^+)$ $(eb)^2$	$g(2_1^+)_{\text{free}}$	$g(2_1^+)_{\text{eff}}$
Experiment			1.461[a]	0.0330(40)[a]	$g_{\text{exp}} = -0.1(1)$[b] $g_{\text{exp}} = -0.015(42)$[c]	
Calculations	A	$(d_{3/2})_\pi^{-2}(f_{7/2})_\nu^2$	0.999	0.0122	−0.441	−0.335
	B	$(d_{3/2})_\pi^{-2}$ (full $fp)_\nu^2$	1.367	0.0174	−0.282	−0.181
	C	$(s_{1/2}, d_{3/2})_\pi^{-2}(f_{7/2})_\nu^2$	0.971	0.0195	−0.335	−0.235
	D	$(s_{1/2}, d_{3/2})_\pi^{-2}$ (full $fp)_\nu^2$	1.328	0.0229	−0.230	−0.129
	E	$(d_{5/2}, s_{1/2}, d_{3/2})_\pi^{-2}$ (full $fp)_\nu^2$	1.431	0.0241	−0.195	−0.104

[a]From Ref. [28].
[b]From Ref. [13].
[c]Present work.

effective g factors used in the preceding calculations are the experimentally measured g factors of the ground states of ^{39}K, $(d_{3/2})_\pi^{-1}$, and ^{41}Ca, $(f_{7/2})_\nu^1$, which differ from the Schmidt values (as is subsequently explained). These authors [13] also reported large-scale shell-model (LSSM) calculations that yielded $g = -0.18(8)$.

The theoretical investigation in the present paper examines the detailed microscopic shell-model structure of the wave function of the 2_1^+ state of ^{40}Ar. For that purpose, calculations utilizing two different interactions, WBT denoted by [27] and FSZM [29] were performed. The single-particle energy spacings utilized with the WBT interaction were $(d_{3/2} - s_{1/2})_\pi = 2.731$ MeV, $(d_{3/2} - d_{5/2})_\pi = 7.418$ MeV, $(p_{3/2} - f_{7/2})_\nu = 1.738$ MeV, $(p_{1/2} - f_{7/2})_\nu = 3.900$ MeV, and $(f_{5/2} - f_{7/2})_\nu = 5.994$ MeV. The single-particle energies appropriate to this interaction are mass dependent [27]. So, for the *fp* neutron shell, the single-particle energies evaluated for ^{41}Ca are used.

Unlike the WBT interaction, the FSZM interaction was not specifically fitted to data in the vicinity of ^{40}Ar. It is introduced here as a counterpoint to WBT just to show that the results do depend on the interaction that is used. The FSZM interaction uses a parametrization of the model space G matrix that was derived by Zheng and Zamick [29] and that has a simple form with two-body central, two-body spin-orbit, and two-body tensor parts. The relevant interaction terms have been adjusted to obtain a good fit to the G-matrix elements for the Bonn A potential. In the present paper, the two-body matrix elements were generated from this interaction with the formula given by Kuo and Brown [30]. The single-particle input energies were modified to fit the experimental low-energy spectra and binding energies of ^{41}Ca and ^{39}K. The single-particle energy spacings utilized were $(d_{3/2} - s_{1/2})_\pi = 2.523$ MeV, $(d_{3/2} - d_{5/2})_\pi = 5$ MeV, $(p_{3/2} - f_{7/2})_\nu = 2$ MeV, $(p_{1/2} - f_{7/2})_\nu = 4$ MeV, and $(f_{5/2} - f_{7/2})_\nu = 6.5$ MeV. The diagonalization of the effective Hamiltonian in large model spaces was achieved by use of the OXBASH program [31,32].

As already mentioned, the g factors of the ground states of ^{39}K and ^{41}Ca differ from the Schmidt values. This effect was largely explained by Mavromatis and Zamick [33] for

TABLE IV. Summary of the shell-model calculations carried out for the 2_1^+ state in ^{40}Ar with the FSZM interaction [29], different model spaces, effective charges $e_\pi = 1.5$, $e_\nu = 0.5$, and either the free nucleon g factors $g(s)_\pi = 5.586$, $g(s)_\nu = -3.826$, $g(l)_\pi = 1$, $g(l)_\nu = 0$, or the effective nucleon g factors $g(s)_\pi = 5.055$, $g(s)_\nu = -3.19$, $g(l)_\pi = 1.06$, $g(l)_\nu = 0$.

		Model space	$E(2_1^+)$ (MeV)	$B(E2; 0_1^+ \to 2_1^+)$ $(eb)^2$	$g(2_1^+)_{\text{free}}$	$g(2_1^+)_{\text{eff}}$
Experiment			1.461[a]	0.0330(40)[a]	$g_{\text{exp}} = -0.1(1)$[b] $g_{\text{exp}} = -0.015(42)$[c]	
Calculations	A	$(d_{3/2})_\pi^{-2}(f_{7/2})_\nu^2$	0.965	0.0134	−0.400	−0.289
	B	$(d_{3/2})_\pi^{-2}$ (full $fp)_\nu^2$	1.424	0.0206	−0.106	+0.007
	C	$(s_{1/2}, d_{3/2})_\pi^{-2}(f_{7/2})_\nu^2$	0.983	0.0240	−0.180	−0.088
	D	$(s_{1/2}, d_{3/2})_\pi^{-2}$ (full $fp)_\nu^2$	1.474	0.0272	−0.023	+0.078
	E	$(d_{5/2}, s_{1/2}, d_{3/2})_\pi^{-2}$ (full $fp)_\nu^2$	1.828	0.0305	+0.026	+0.103

[a]From Ref. [28].
[b]From Ref. [13].
[c]Present work.

TABLE V. Calculations of the ground state g factors of ^{39}K($3/2^+$) ($g_{\rm exp} = 0.26098(2)$ [36]), ^{41}Ca($7/2^+$) ($g_{\rm exp} = -0.455652(3)$ [36]) and ^{40}K(4^-) ($g_{\rm exp} = -0.324525(1)$ [36]) carried out with the WBT [27] and FSZM interactions [29], different model spaces, and with free and effective (see text) nucleon g factors.

Nucleus	Model space	$g_{\rm free}^{\rm WBT}$	$g_{\rm free}^{\rm FSZM}$	$g_{\rm eff}^{\rm WBT}$	$g_{\rm eff}^{\rm FSZM}$
^{39}K	$(d_{3/2})_\pi^{-1}$	0.083	0.083	0.261	0.261
^{39}K	(full sd)$^{-1,-3}$ (full fp)^{0,2}	0.067	0.060	0.248	0.234
^{41}Ca	$(f_{7/2})_\nu^1$	−0.546	−0.546	−0.456	−0.456
^{41}Ca	(full sd)$^{0,-2}$ (full fp)^{1,3}	−0.538	−0.526	−0.447	−0.435
^{40}K	(full sd)$_\pi^{-1}$ (full fp)$_\nu^1$	−0.427	−0.445	−0.318	−0.334
^{40}K	(full sd)$^{-1,-3}$ (full sd)^{1,3}	−0.421	−0.425	−0.312	−0.315

these two particular nuclei on the basis of second-order perturbation theory. However, these authors note that, more generally, second-order configuration mixing corrections must be considered alongside exchange currents, spin-orbit, and relativistic corrections. More detailed calculations by Towner [34] include renormalizations of g_l as well as of g_s.

Tables III and IV summarize the results of the ^{40}Ar calculations in several model spaces, with the WBT [27] and FSZM [29] interactions, respectively, for $E(2_1^+)$, $B(E2; 0_1^+ \rightarrow 2_1^+)$, and $g(2_1^+)$ both with free and with effective nucleon g factors. The effective nucleon g factors of $g(s)_\nu = -3.19$ and $g(l)_\nu = 0.0$, evaluated for the fp shell and the KB1 interaction in Ref. [2], were chosen for the neutrons, because of their best fit to the ground state g factor of ^{41}Ca (Table V). For the sd protons, $g(l)_\pi = 1.06$ and $g(s)_\pi = 5.055$, adjusted to fit the ground state g factor of ^{39}K in a simple $\pi d_{3/2}^{-1}$ configuration, were used (Table V). The Brown and Wildenthal [35] effective g factors of $g(s)_\pi = 4.66$ and $g(l)_\pi = 1.143$, as evaluated for the sd shell, overestimate the ground state g factor of ^{39}K (0.045 as compared with the experimental value of 0.026). The values of Towner [34] give a good result for ^{39}K, but do not appreciably change the g factor of ^{41}Ca from its Schmidt value because of a cancellation between the corrective effect of spin renormaliztion and the opposite effect of orbital renormalization—the latter coming mainly from exchange currents.

It is shown in Table V that the experimental ground state g factor of $^{40}_{19}$K$_{21}$ is also well reproduced, for both interactions, with the effective nucleon g factors that are used in this paper, but not with the free nucleon g factors. The g values obtained in the large model spaces (which include also the possibility of two-particle two-hole excitations) given in Table V for ^{39}K and ^{41}Ca show very small differences from the results obtained with the one-hole and one-particle configurations, respectively. The results with the effective nucleon g factors for ^{40}Ar are shown in the last column of Tables III and IV. For all the cases, in both tables, the use of effective g factors results in less negative or more positive $g(2_1^+, ^{40}\text{Ar})$. Except for cases A, the g factors calculated with the FSZM interaction and the free nucleon g factors are less negative than those calculated with the WBT interaction and effective nucleon g factors. Therefore, overall, the FSZM interaction produces less negative g factors than does the WBT interaction.

A comparison of the results from calculations A and C, as well as from B and D, in Tables III and IV, reveals that the inclusion of the $(s_{1/2})_\pi$ orbital produces a larger change in the g factor for the FSZM interaction than for the WBT interaction. Consequently the $(s_{1/2})_\pi$ orbital seems to play a bigger role with the FSZM interaction than with the WBT interaction. The addition of the $(d_{5/2})_\pi$ orbital to the model space (calculations E) changes the final g-factor results with both interactions by about the same amount. However, the calculated excitation energy with the FSZM interaction (but not the WBT), in model space E, (full $sd)_\pi$ (full $fp)_\nu$, is larger than the experimental value, hinting that the final g factor result may also be overestimated. Furthermore, with the FSZM interaction, a $B(E2)$ value closer to the experimental result is obtained.

The probabilities of the different components (>1%) of the (2_1^+,^{40}Ar) wave function for configuration E with the WBT and the FSZM interactions are displayed in Table VI together with the corresponding g factors for each component. It can be seen that a good approximation to the results of calculation E, with both interactions, for $g(2_1^+, ^{40}\text{Ar})$ with effective g factors can be obtained by considering just the first two components in Table VI. For the WBT interaction

TABLE VI. The probability of each wave function component of the 2_1^+ state of ^{40}Ar as obtained from calculations in the (full $sd)_\pi^{-2}$(full $fp)_\nu^2$ space, with effective nucleon g factors, and with the FSZM and the WBT interactions. Only components with a probability contribution of more than 1% are included. The g factor of each component configuration, coupled to 2^+, is given in the last column.

Configuration	Contribution (FSZM) (%)	$g_{\rm eff}$ (FSZM)	Contribution (WBT) (%)	$g_{\rm eff}$ (WBT)
$(d_{3/2}^{-2})_\pi(f_{7/2}^2)_\nu$	48.2	−0.289	72.3	−0.335
$(s_{1/2}^{-1}d_{3/2}^{-1})_\pi(f_{7/2}^2)_\nu$	15.3	+1.326	8.1	+1.361
$(s_{1/2}^{-2})_\pi(f_{7/2}^2)_\nu$	8.4	−0.457	2.8	−0.456
$(d_{5/2}^{-2})_\pi(f_{7/2}^2)_\nu$	6.8	+0.233	2.1	+0.191
$(d_{5/2}^{-1}s_{1/2}^{-1})_\pi(f_{7/2}^2)_\nu$	3.9	+1.152		
$(d_{3/2}^{-2})_\pi(f_{7/2}^1p_{3/2}^1)_\nu$	3.8	−0.120	7.0	−0.124
$(d_{3/2}^{-2})_\pi(p_{3/2}^2)_\nu$	3.0	−0.151	2.2	−0.943
$(d_{5/2}^{-1}d_{3/2}^{-1})_\pi(f_{7/2}^2)_\nu$	2.4	+2.153		
$(d_{3/2}^{-2})_\pi(f_{5/2}^2)_\nu$	1.5	+0.387	1.2	+0.421

these components yield -0.242 and $+0.110$, respectively, adding to -0.132, close to the -0.104 in Table III. For the FSZM interaction the corresponding results are -0.139 and $+0.203$, adding to $+0.064$, close to the $+0.103$ in Table IV. An important difference between the wave functions predicted by the two interactions is the relatively greater dominance in the probability of the first component for WBT ($\approx$72%) compared with the probability of the first component for FSZM ($\approx$48%). Although the most obvious difference in the two interactions seems to be the $(d_{3/2} - d_{5/2})_\pi$ splitting, the main reason the results are different is actually due to the amount of $s_{1/2} - d_{3/2}$ mixing in the wave function, as was also concluded above from a comparison of Tables III and IV. The occupation of the $d_{5/2}$ orbital is also larger with the WBT interaction than with the FSZM interaction, but its inclusion does not seem to produce a significant difference in the final g-factor results with either interaction (see Tables III and IV). With effective g factors, the WBT interaction yields $g(2_1^+) = -0.104$ and the FSZM interaction yields $g(2_1^+) = +0.103$, whereas the experimental g factor lies in between. The experimental error, the somewhat different results obtained with the two interactions, as well as the uncertainties in both the single-particle energies and in the effective nucleon g factors, all suggest that detailed quantitative comparisons of the calculations with the experimental results are difficult.

It must be emphasized that no explicit core excitations were included in any calculations of ^{40}Ar. Some amount of implicit core admixtures may be taken into account when effective g factors are used. A comparison of the results obtained with either small or very large model spaces for ^{39}K, ^{40}Ca, and ^{41}K in Table V suggests that the core-excitation admixtures are relatively small. In the ^{40}Ar isotone ^{42}Ca a deformed component, which is due to core excitations, of about 55% was estimated for the 2_1^+ state [7,37,38]. ^{40}Ar and ^{42}Ca have similar $B(E2; 2_1^+ \rightarrow 0_1^+)$ values of 9.3(4) W.u. [28] and 7.5(5) W.u. [7], respectively, results that depend on the nature of both the 0_1^+ and 2_1^+ states. Nevertheless, the calculations performed with the FSZM interaction suggest that core excitations do not play a role in the structure of the ^{40}Ar(2_1^+) state. On the other hand, the result of calculation E with the WBT interaction and the effective nucleon g factors, combined with the approach of Ref. [9], results in a deformed core-excited component of about 16(8)%. Clearly, excitations from the core play a much smaller role in the ^{40}Ar 2_1^+ state than in the ^{42}Ca 2_1^+ state and a near-spherical shell-model wave function, with at most a small core-excited component, may describe adequately the ^{40}Ar 2_1^+ state. More extensive calculations and more precise measurements are needed to reveal the quantitative contribution, if any, of core excitations to the structure of ^{40}Ar(2_1^+) state and to explain why ^{40}Ar differs from ^{42}Ca. Small collectivity was also concluded [39] for the Ar isotopes between $N = 20$ and $N = 28$, based on the LSSM calculations, within the (full $sd)_\pi$ (full $fp)_\nu$ model space, for the 2_1^+ excitation energies and the experimental two-neutron separation energy. The experimentally measured quadrupole moments $Q[^{40}\text{Ar}(2_1^+)] = +0.01(4)$ [40] and $Q[^{42}\text{Ca}(2_1^+)] = -0.19(8)$ [10] also support the arguments made above about the different nature of the 2_1^+ states in these two nuclei.

VI. SUMMARY

The g factor of the 2_1^+ state in ^{40}Ar, $g = -0.015(42)$, was remeasured with a greater accuracy by the transient field technique and Coulomb excitation of the beam in inverse kinematics. This result agrees, within the errors of the measurement, with $g = -0.1(1)$ measured previously at very high velocities [13].

In ^{42}Ca, the isotone of ^{40}Ar, it was necessary to involve significant core excitation in order to explain its positive $g(2_1^+)$ factor [7]. In contrast, in ^{40}Ar, shell-model calculations with the FSZM interaction and within the (full $sd)_\pi$(full $fp)_\nu$ model space, without including core excitations, are sufficient to describe the properties of the 2_1^+ state. The same calculations with the WBT interaction are compatible with a core-excitation component that is much smaller than that in ^{42}Ca. In summary, this paper shows that the 2_1^+ states in ^{42}Ca and ^{40}Ar have a different nature and that a near-spherical shell-model picture may be assumed for the ^{40}Ar 2_1^+ state.

ACKNOWLEDGMENTS

The authors are indebted to the staff of the Lawrence Berkeley National Laboratory 88-Inch Cyclotron. The target used in this experiment was prepared by P. Maier-Komor, Physik-Department der Technischen Universität München, D-85748 Garching, Germany. We are grateful to B. A. Brown for useful suggestions and for sharing the updated version of the OXBASH code. A helpful communication from I. S. Towner is gratefully acknowledged. S.J.Q.R. would like to acknowledge travel support from the University of Southern Indiana. Y.Y.S. is grateful for a Stockton College Summer Research Award. M.J.T. acknowledges travel support from Rutgers University. The work was supported in part by the U.S. National Science Foundation under NSF grants PHY-98800 for Rutgers University and the U.S. Department of Energy contracts DE-AC03-76SF0098 and DE-AC02-98CH10886 for the University of California, Lawrence Berkeley National Laboratory and W-7405-Eng-48 for Lawrence Livermore National Laboratory. Support from the U.S. Department of Energy grant DE-FG02-95ER-40940 is acknowledged.

[1] E. K. Warburton, C. W. Beausang, D. B. Fossan, L. Hildingsson, W. F. Piel, and J. A. Becker, Phys. Rev. C **34**, 136 (1986).

[2] W. Richter, M. van der Merwe, R. Julies, and B. Brown, Nucl. Phys. **A523**, 325 (1991).

[3] M. van der Merwe, W. Richter, and B. Brown, Nucl. Phys. **A579**, 173 (1994).

[4] E. Caurier, G. Martinez-Pinedo, F. Nowacki, A. Poves, J. Retamosa, and A. P. Zuker, Phys. Rev. C **59**, 2033 (1999).

[5] J. Gomez, K. Kar, V. Kota, R. Molina, and J. Retamosa, Phys. Lett. **B567**, 251 (2003).
[6] A. A. Raduta, L. Zamick, E. Moya de Guerra, A. Faessler, and P. Sarriguren, Phys. Rev. C **68**, 044317 (2003).
[7] S. Schielke, D. Hohn, K.-H. Speidel, O. Kenn, J. Leske, N. Gemein, M. Offer, J. Gerber, P. Maier-Komor, and O. Zell *et al*., Phys. Lett. **B571**, 29 (2003).
[8] M. J. Taylor, N. Benczer-Koller, G. Kumbartzki, T. J. Merzimekis, S. J. Q. Robinson, Y. Y. Sharon, L. Zamick, A. E. Stuchbery, C. Hutter, and C. W. Beausang *et al*., Phys. Lett. **B559**, 187 (2003).
[9] W. J. Gerace and A. M. Green, Nucl. Phys. **A93**, 110 (1967).
[10] C. W. Towsley, D. Cline, and R. N. Horoshko, Nucl. Phys. **A204**, 574 (1973).
[11] K.-H. Speidel, S. Schielke, O. Kenn, J. Leske, D. Hohn, H. Hodde, J. Gerber, P. Maier-Komor, O. Zell, and Y. Y. Sharon *et al*., Phys. Rev. C **68**, 061302(R) (2003).
[12] M. J. Taylor, N. Benczer-Koller, L. Bernstein, J. Cooper, K. Hiles, D. S. Judson, G. Kumbartzki, P. Maier-Komor, M. A. McMahan, and T. J. Merzimekis *et al*. Phys. Lett. **B605**, 265 (2005).
[13] J. Cub, U. Knopp, K.-H. Speidel, H. Bush, S. Kremeyer, H.-J. Wollersheim, N. Martin, X. Hong, K. Vetter, and N. Gollwitzer *et al*., Nucl. Phys. **A549**, 304 (1992).
[14] K.-H. Speidel, N. Benczer-Koller, G. Kumbartzki, C. Barton, A. Gelberg, J. Holden, G. Jakob, N. Matt, R. H. Mayer, and M. Satteson *et al*., Phys. Rev. C **57**, 2181 (1998).
[15] J. Holden, N. Benczer-Koller, G. Jakob, G. Kumbartzki, T. J. Mertzimekis, K.-H. Speidel, C. W. Beausang, R. Krücken, A. Macchiavelli, and M. McMahan *et al*., Phys. Rev. C **63**, 024315 (2001).
[16] T. J. Mertzimekis, N. Benczer-Koller, J. Holden, G. Jakob, G. Kumbartzki, K.-H. Speidel, R. Ernst, A. Macchiavelli, M. McMahan, and L. Phair *et al*., Phys. Rev. C **64**, 024314 (2001).
[17] P. Maier-Komor, K.-H. Speidel, and A. Stolarz, Nucl. Instrum. Methods Phys. Res. A **334**, 191 (1993).
[18] A. Piqué, J. M. Brennan, R. Darling, R. Tanczyn, D. Ballon, and N. Benczer-Koller, Nucl. Instrum. Methods Phys. Res. **A279**, 579 (1989).
[19] J. F. Ziegler, J. Biersack, and U. Littmark, *The Stopping and Range of Ions in Solids* (Pergamon, Oxford, 1985), Vol. 1.
[20] P. Endt, Nucl. Phys. **A633**, 1 (1998).
[21] A. Winther and J. de Boer, in *Coulomb Excitation*, edited by K. Alder and A. Winther (Academic, New York, 1966), pp. 303–374.
[22] J. A. Cameron, M. A. Bentley, A. M. Bruce, R. A. Cunningham, W. Gelletly, H. G. Price, J. Simpson, D. D. Warner, and A. N. James, Phys. Rev. C **49**, 1347 (1994).
[23] R. Ernst, K.-H. Speidel, O. Kenn, A. Gohla, U. Nachum, J. Gerber, P. Maier-Komor, N. Benczer-Koller, G. Kumbartzki, and G. Jakob *et al*., Phys. Rev. C **62**, 024305 (2000).
[24] N. K. B. Shu, D. Melnik, J. M. Brennan, W. Semmler, and N. Benczer-Koller, Phys. Rev. C **21**, 1828 (1980).
[25] R. Ernst, K.-H. Speidel, O. Kenn, U. Nachum, J. Gerber, P. Maier-Komor, N. Benczer-Koller, G. Jakob, G. Kumbartzki, and L. Zamick *et al*., Phys. Rev. Lett. **84**, 416 (2000).
[26] N. K. B. Shu, R. Levy, N. Tsoupas, W. Andrejtscheff, A. Lopez-Garcia, A. Stuchbery, H. H. Bolotin, and N. Benczer-Koller, Hyperfine Interact. **9**, 65 (1981).
[27] E. K. Warburton and B. A. Brown, Phys. Rev. C **46**, 923 (1992).
[28] S. Raman, C. W. Nestor, Jr., and P. Tikkanen, At. Data Nucl. Data Tables **78**, 1 (2001).
[29] D. C. Zheng and L. Zamick, Ann. Phys. (NY) **206**, 106 (1991).
[30] T. Kuo and G. Brown, Nucl. Phys. **85**, 40 (1966).
[31] B. A. Brown, A. Etchegoyen, N. S. Godwin, W. D. Rae, W. A. Richter, W. E. Ormand, E. K. Warburton, J. S. Winfield, L. Zhao, and C. H. Zimmerman, OXBASH, MSU-NSCL Report No. 524.
[32] B. A. Brown (private communication).
[33] H. A. Mavromatis and L. Zamick, Phys. Lett. **20**, 171 (1966).
[34] I. S. Towner, Phys. Rep. **155**, 263 (1987).
[35] B. A. Brown and B. H. Wildenthal, Nucl. Phys. **A474**, 290 (1987).
[36] P. Raghavan, At. Nucl. Data Tables **42**, 189 (1989).
[37] N. Benczer-Koller, M. J. Taylor, G. Kumbartzki, Y. Y. Sharon, L. Zamick, T. J. Mertzimekis, and A. E. Stuchbery, in *Symmetries in Nuclear Structure* (World Scientific Publishing Co., Singapore, 2003), p. 325.
[38] N. Benczer-Koller, G. Kumbartzki, T. J. Mertzimekis, Y. Y. Sharon, K.-H. Speidel, M. J. Taylor, and L. Zamick, in *Nuclear Physics, Large and Small: International Conference on Microscopic Studies of Collective Phenomena* (American Institue of Physics, New York, 2004), p. 81.
[39] J. Retamosa, E. Caurier, F. Nowacki, and A. Poves, Phys. Rev. C **55**, 1266 (1997).
[40] K. Nakai, J. Québert, F. Stephens, and R. Diamond, Phys. Rev. Lett. **24**, 903 (1970).